J. Fluid Mech. (2012), *vol.* 711, *pp.* 27–39. © Cambridge University Press 2012
doi:10.1017/jfm.2012.360

Linear stability analysis of cylindrical Rayleigh–Bénard convection

Bo-Fu Wang[1], Dong-Jun Ma[2], Cheng Chen[3] and De-Jun Sun[1]†

[1] Department of Modern Mechanics, University of Science and Technology of China, Hefei 230027, China

[2] School of Aerospace Engineering, Georgia Institute of Technology, Atlanta, GA 30332, USA

[3] Low Speed Aerodynamics Institute, China Aerodynamics Research and Development Center, Mianyang, Sichuan 622762, China

(Received 1 January 2012; revised 18 April 2012; accepted 12 July 2012; first published online 13 September 2012)

The instabilities and transitions of flow in a vertical cylindrical cavity with heated bottom, cooled top and insulated sidewall are investigated by linear stability analysis. The stability boundaries for the axisymmetric flow are derived for Prandtl numbers from 0.02 to 1, for aspect ratio A ($A = H/R =$ height/radius) equal to 1, 0.9, 0.8, 0.7, respectively. We found that there still exists stable non-trivial axisymmetric flow beyond the second bifurcation in certain ranges of Prandtl number for $A = 1$, 0.9 and 0.8, excluding the $A = 0.7$ case. The finding for $A = 0.7$ is that very frequent changes of critical mode (azimuthal Fourier mode) of the second bifurcation occur when the Prandtl number is changed, where five kinds of steady modes $m = 1, 2, 8, 9, 10$ and three kinds of oscillatory modes $m = 3, 4, 6$ are presented. These multiple modes indicate different flow structures triggered at the transitions. The instability mechanism of the flow is explained by kinetic energy transfer analysis, which shows that the radial or axial shear of base flow combined with buoyancy mechanism leads to the instability results.

Key words: bifurcation, buoyancy-driven instability, convection in cavities

1. Introduction

Cylindrical Rayleigh–Bénard convection is a classical prototype of pattern formation (Cross & Hohenberg 1993). This system has been the focus of intensive studies because of its theoretical and practical importance (Bodenschatz, Pesch & Ahlers 2000). The flow instabilities in the convection play a crucial role in how the convection patterns develop. The instability of the conductive state has been well established since the works of Charlson & Sani (1970, 1971), Stork & Müller (1975), Rosenblat (1982) and Buell & Catton (1983). All these works have shown that flow structure after the primary threshold is independent of the Prandtl number but depends on the aspect ratio A. The transition between axisymmetric and non-axisymmetric modes occurs around $A = 1.44$ for conductive sidewalls. The flow is axisymmetric ($m = 0$) for $0.64 < A < 1.1$ and non-axisymmetric ($m = 1$) for larger values of A in the case of adiabatic sidewalls. The critical Rayleigh number decreases asymptotically towards a constant value as $A \to 0$.

† Email address for correspondence: dsun@ustc.edu.cn

The stability of the first convective state depending on both aspect ratio and Prandtl number has been investigated mainly for axisymmetric primary flow. The first numerical investigation of the instability of the axisymmetric flows at small aspect ratios is due to Charlson & Sani (1975). However, they failed to predict the secondary instability satisfactorily, since the resolution available at that time was inadequate and the mode truncation was too severe. Müller, Neumann & Weber (1984) investigated convective flows experimentally and numerically for $Pr = 0.02$ and $Pr = 6.7$. They observed axisymmetric flows for $A = 1$ and non-axisymmetric flows for $2 < A < 10$. They also found numerically a second stable solution at $Ra = 2800$ with symmetry $m = 2$, which agrees with the result reported by Neumann (1990). Hardin & Sani (1993) calculated weakly nonlinear solutions to the Boussinesq equations for several moderate and large aspect ratios. They corrected some results of Charlson & Sani (1975) and extended them for convection with the Soret effect. Very recently, Hért *et al.* (2010) experimentally studied both conductive and convective instability in cylindrical convection for $0.22 < A < 2$ and $Pr = 28.9$. Most of their results are consistent with previous stability analysis and numerical simulations.

Wanschura, Kuhlmann & Rath (1996) performed a numerical study of secondary convective instabilities for moderate-aspect-ratio cylinders. The study was done in the aspect ratio range $0.64 < A < 1.1$, for which the primary threshold corresponds to the axisymmetric mode $m = 0$. The Prandtl number is fixed at two values: $Pr = 0.02$ and $Pr = 1$. The secondary threshold increases with the Prandtl number, and also strongly depends on the aspect ratio. The unstable mode of this secondary transition corresponds to the $m = 2$ mode in general, while oscillatory $m = 3$ and $m = 4$ modes are also observed in a narrow aspect ratio $0.64 < A < 0.69$ at $Pr = 1$. They also elucidated the instability mechanism by energy analysis. The axisymmetric flow becomes unstable due to the classical thermal instability mechanism for large Prandtl numbers, whereas for small Prandtl numbers the secondary instability is inertial in nature. Touihri, Ben Hadid & Henry (1999) numerically investigated the stability of the conductive state for aspect ratios $A = 1$ and $A = 2$ and the convective state for $A = 1$. They established a diagram of primary bifurcations, including unstable branches. The secondary bifurcation point for $A = 1$ and $0 < Pr < 1$ has also been given. Borońska & Tuckerman (2006) performed a more detailed description of the oscillatory instability with the azimuthal wavenumbers $m = 3$ and $m = 4$ found by Wanschura *et al.* (1996). The transitions from steady axisymmetric flows to time-dependent flows are studied by nonlinear simulations, linear stability analysis and bifurcation theory. Their results demonstrate that the axisymmetric flow becomes unstable to standing and travelling azimuthal waves at a Rayleigh number near 7400, and the standing waves are slightly unstable to travelling waves. Moreover, they interpreted their results as a Hopf bifurcation in a system with $O(2)$ symmetry.

An interesting experimental study was carried out by Hof, Lucas & Mullin (1999). They observed five distinct steady patterns for fixed $A = 0.5$, $Pr = 6.7$ and $Ra = 1775$ with insulating sidewalls. They also reported a transition from an axisymmetric steady state towards the azimuthal waves. There are some further simulations and analyses relevant to this experiment. Rüdiger & Feudel (2000) numerically studied the formation of different patterns as straight rolls, targets, and spirals in a cylindrical system for $A = 0.25$ and $Pr = 1$. Leong (2002) used a finite difference method to simulate convective flows for $Pr = 7$ in cylinders of aspect ratios $A = 0.25$ and 0.5 with adiabatic lateral walls. They observed several steady patterns of parallel rolls, three-spoke flow and axisymmetric state, all of which were stable in the range $781 < Ra < 4688$. Ma, Sun & Yin (2006) numerically studied the flow state

multiplicity in Hof *et al.* (1999) under the same parameters. Very recently, Borońska & Tuckerman (2010*a*,*b*) performed a more complete survey of the convective patterns at the parameter $A = 0.5$ and $Pr = 6.7$ by numerical and bifurcation analysis for both insulating and conductive sidewalls.

Based on the second instability analysis of Wanschura *et al.* (1996) and Touihri *et al.* (1999), the present study concerns not only the stability of axisymmetric flow corresponding to the second bifurcation but also the stability of axisymmetric flow beyond the second bifurcation. Several parameter variations are performed to obtain deeper insights into the nature of the convective instability. The influences of geometry (aspect ratio) and physical parameters (Prandtl number) are studied systematically by linear stability analysis. Further, the kinetic energy transfer between the basic state and a disturbance is considered in order to elucidate the instability mechanisms.

2. Problem formulation and numerical method

We consider an incompressible Newtonian fluid confined in a vertical cylindrical cavity of aspect ratio $A = H/R$, where H is the height and R is the radius of the cavity. The cylinder is uniformly heated from below with a higher temperature T_h and cooled from above with a lower temperature T_c, whereas the sidewall is adiabatic. In cylindrical coordinates, the domain is $(r, \varphi, z) \in [0, 1] \times [0, 2\pi] \times [0, A]$. The three-dimensional problem is described by the Boussinesq equations. All the physical characteristics are taken as constant except the density, which is taken as a linear function of temperature in the buoyancy term, $\rho = \rho_0[1 - \alpha(T - T_0)]$, where α is the thermal expansion coefficient and T_0 is the reference temperature ($T_0 = T_c$). The length, time, velocity and pressure are scaled by R, R^2/κ, κ/R, and $\rho\,(\kappa/R)^2$, respectively, where κ is the thermal diffusivity. Non-dimensional temperature is defined by $\Theta = (T - T_c)/(T_h - T_c)$. The dimensionless governing equations can be written as

$$\nabla \cdot \boldsymbol{u} = 0, \tag{2.1}$$

$$\frac{\partial \boldsymbol{u}}{\partial t} + \boldsymbol{u} \cdot \nabla \boldsymbol{u} = -\nabla p + Pr\,\nabla^2 \boldsymbol{u} + PrRa\Theta\hat{\boldsymbol{z}}, \tag{2.2}$$

$$\frac{\partial \Theta}{\partial t} + \boldsymbol{u} \cdot \nabla \Theta = \nabla^2 \Theta, \tag{2.3}$$

where $Pr = \nu/\kappa$ is the Prandtl number, ν is the kinematic viscosity, $Ra = g\alpha(T_h - T_c)R^3/(\kappa\nu)$ is the Rayleigh number, g is the gravity acceleration, and $\hat{\boldsymbol{z}}$ is the unit vector in the z direction.

The boundary conditions for velocity and temperature are

$$\boldsymbol{u} = 0 \quad \text{for } r = 1 \text{ or } z = 0, A, \tag{2.4}$$

$$\frac{\partial \Theta}{\partial r} = 0 \quad \text{for } r = 1, \tag{2.5}$$

$$\Theta = 1 \quad \text{for } z = 0, \quad \Theta = 0 \quad \text{for } z = A. \tag{2.6}$$

Setting $\boldsymbol{u} = 0$ for the whole field, we can obtain the temperature distribution for the diffusive motionless state, $\Theta(z) = (1 - z/A)$.

The governing equations (2.1)–(2.3) have been solved using second-order centre differences in space and a second-order fractional-step method in time in three-dimensional cylindrical coordinates, which is an improved version of the algorithm in Verzicco & Orlandi (1996) and Ma *et al.* (2006). An additional pressure predictor

as in Hugues & Randriamampianina (1998) is employed before each time step. The numerical results show that the new method is more robust than the original steady-state solver using Newton's method.

A Jacobian-free Newton–Krylov method (JFNK) (Knoll & Keyes 2004) is implemented to capture the stable and unstable steady-state solution, which is the basis of linear stability analysis. We have used the first-order implicit/explicit Euler scheme for the calculation of a Stokes preconditioner that allows a matrix-free inversion of the preconditioned Jacobian needed in each Newton iteration (Tuckerman & Barkley 2000). The corresponding linear system is solved by an iterative technique using the BiCGstab algorithm (van der Vorst 1992); with this method the Jacobian matrix is never constructed or stored.

The linear stability of steady state $\boldsymbol{u}$ is governed by the eigenvalues λ_j of the Jacobian $(\boldsymbol{N}_{\boldsymbol{u}} + \boldsymbol{L})$:

$$(\boldsymbol{N}_{\boldsymbol{u}} + \boldsymbol{L})\boldsymbol{u}' = \lambda \boldsymbol{u}'. \tag{2.7}$$

This follows from the fact that infinitesimal perturbations from a steady state evolve according to the linear stability equation

$$\partial_t \boldsymbol{u}' = (\boldsymbol{N}_{\boldsymbol{u}} + \boldsymbol{L})\boldsymbol{u}'. \tag{2.8}$$

The implicitly restarted Arnoldi method (Lehoucq, Sorensen & Yang 1998) using ARPACK routines is implemented to calculate the leading eigenvalues. By time-stepping the linearized equations, we are able to construct a small matrix which represents the action of the Jacobian $\boldsymbol{J}$ on the subspace of the leading eigenvectors. Diagonalization of this matrix gives the leading eigenvalues and eigenvectors.

Our code was successfully tested by comparison with results of Buell & Catton (1983), Touihri *et al.* (1999) and Borońska & Tuckerman (2006). Most of our simulations were performed using a grid $70 \times 90 \times 60$ in the radial, azimuthal and vertical directions respectively.

In order to get some physical insights into the stability results, we performed the kinetic energy transfer analysis around selected critical points. The total kinetic change rate is given by the Reynolds–Orr equation obtained by multiplying (2.8) by $\boldsymbol{u}'$ and integrating over the volume Ω occupied by the fluid (Ma, Henry & Ben Hadid 2005). The rate of kinetic change $\mathrm{d}K/\mathrm{d}t$ can be written as

$$\begin{aligned}
\frac{\mathrm{d}K}{\mathrm{d}t} &= \frac{\mathrm{d}}{\mathrm{d}t}\int_\Omega \frac{1}{2}\boldsymbol{u}'\boldsymbol{u}'\,\mathrm{d}\Omega = -\int_\Omega \boldsymbol{u}'\cdot(\boldsymbol{u}'\cdot\boldsymbol{\nabla}\boldsymbol{u})\,\mathrm{d}\Omega \\
&\quad - Pr\int_\Omega (\boldsymbol{\nabla}\times\boldsymbol{u}')^2\,\mathrm{d}\Omega + PrRa\int_\Omega u_z'\Theta'\,\mathrm{d}\Omega \\
&= -\int_\Omega \left(u_r'u_r'\frac{\partial u_r}{\partial r} + u_r'u_z'\frac{\partial u_r}{\partial z} + u_z'u_r'\frac{\partial u_z}{\partial r} + u_z'u_z'\frac{\partial u_z}{\partial z} + \frac{u_\varphi'u_\varphi'u_r}{r}\right)\mathrm{d}\Omega \\
&\quad - Pr\int_\Omega (\boldsymbol{\nabla}\times\boldsymbol{u}')^2\,\mathrm{d}\Omega + PrRa\int_\Omega u_z'\Theta'\,\mathrm{d}\Omega \\
&= K_v + K_d + K_b \\
&= K_{v1} + K_{v2} + K_{v3} + K_{v4} + K_{v5} + K_d + K_b,
\end{aligned} \tag{2.9}$$

where K_v is the interaction between the disturbance $\boldsymbol{u}'$ and the basic flow $\boldsymbol{u}$, and K_d and K_b represent the viscous dissipation of the perturbation kinetic energy and buoyancy forces, respectively. The terms on the right-hand side of (2.9) with a positive (negative) sign destabilize (stabilize) the base flow. The sign and magnitude of K_v

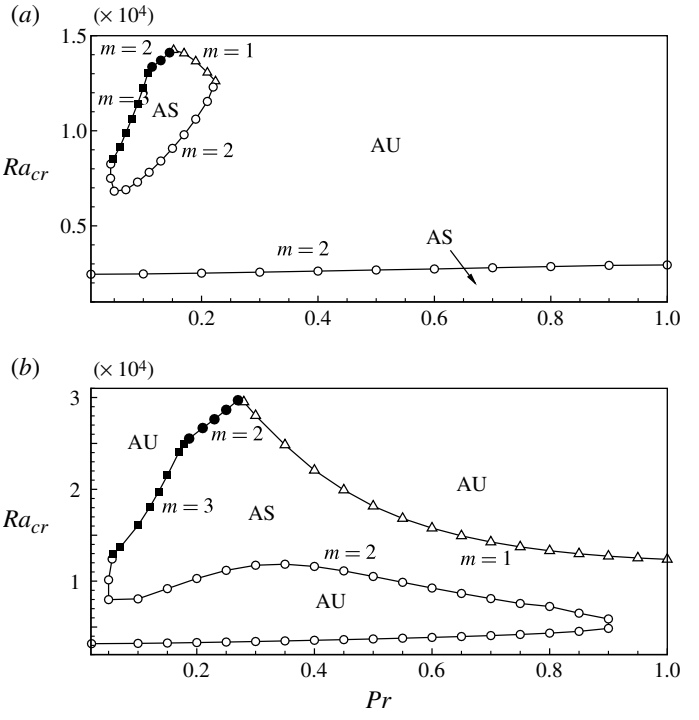

FIGURE 1. Stability curves for the three-dimensional instability of the axisymmetric basic flow: (*a*) $A = 1$; (*b*) $A = 0.9$. Solid curves with hollow symbols represent steady transitions and solid symbols oscillatory transitions. Up triangles (△), $m = 1$ modes at the transition; circles (○), $m = 2$ modes; solid circles (●), $m = 2$ modes; solid squares (■), $m = 3$ modes. The AS in the figures indicates the region in which the axisymmetric flow is stable, and AU means there is no stable axisymmetric base flow in the region.

depend sensitively on both the critical mode and the basic state: it includes both stabilizing and destabilizing effects. As K_d is negative, it is stabilizing.

3. Results

The primary flow in a cylindrical Rayleigh–Bénard system is quiescent: it bifurcates to convective axisymmetric flow, which breaks the Boussinesq symmetry in the axial direction with increasing Rayleigh number in our studied parameter region. The axisymmetric flow will further bifurcate to a three-dimensional flow, which breaks the azimuthal symmetry. The variations of the critical Rayleigh number and critical frequency are plotted as functions of Pr for aspect ratios $A = 1, 0.9, 0.8, 0.7$. Kinetic energy transfer analysis has been performed to investigate the physical mechanisms.

3.1. *Stability results*

Figures 1 and 2 give the stability diagrams for each aspect ratio. The stability result for $A = 1$ is shown in figure 1(*a*). The lower curve in figure 1(*a*) corresponds to the critical Rayleigh number for the second bifurcation to the steady $m = 2$ mode, which is consistent with the result of Touihri *et al.* (1999). Beyond the second bifurcation, we found that there still exists stable axisymmetric flow for $0.044 < Pr < 0.226$ in certain Rayleigh number ranges, which was not mentioned in Touihri *et al.* (1999).

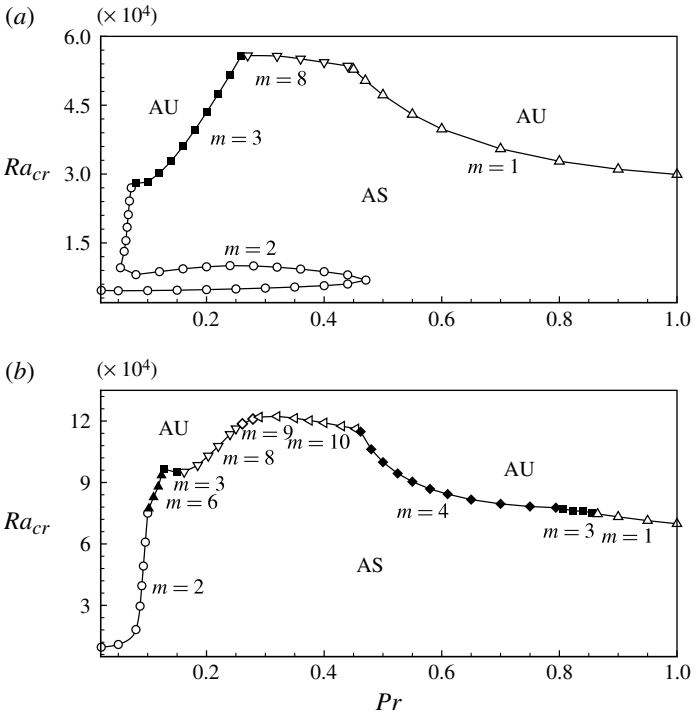

FIGURE 2. Stability curves for the three-dimensional instability of the axisymmetric basic flow: (*a*) $A = 0.8$; (*b*) $A = 0.7$. Solid curves with hollow symbols represent steady transitions and solid symbols oscillatory transitions. Up triangles (△), $m = 1$ modes at the transition; circles (○), $m = 2$ modes; down triangles (▽), $m = 8$ modes; diamonds (◇), $m = 9$ modes; left triangles (◁), $m = 10$ modes; solid circles (●), $m = 2$ modes; solid squares (■), $m = 3$ modes; solid diamonds (◆), $m = 4$ modes; solid up triangles (▲), $m = 6$ modes. The AS in the figures indicates the region in which the axisymmetric flow is stable, and AU means there is no stable axisymmetric base flow in the region.

The axisymmetric flow is calculated by direct numerical simulation and taken as the base flow for linear instability analysis. The instability boundary of the axisymmetric flow is determined by the instability analysis with either decreasing or increasing *Ra*. It is shown in figure 1(*a*) that the critical points form a closed curve. The region in which the axisymmetric flow is stable (AS) and the region in which the axisymmetric flow is always unstable (AU) are divided by the stability curves. If the parameter (*Pr*, *Ra*) lies in the AS region, the flow can be axisymmetric; otherwise the flow will be three-dimensional. Taking the axisymmetric flow in the closed region as the base flow, a decrease in *Ra* will cause a steady $m = 2$ flow, which is similar to the flow beyond the second bifurcation. Meanwhile, an increase in *Ra* will lead to multiple transitions to steady or oscillatory flows, depending on the Prandtl number. First, for an extremely narrow range of *Pr* around 0.044, the transition is through a steady $m = 2$ bifurcation. Then the wavenumber of the leading mode varies continuously from oscillatory for $m = 3$ to oscillatory for $m = 2$ and to steady for $m = 1$.

The stability analyses for smaller aspect ratios were performed in order to evaluate the effect of aspect ratio. Figures 1(*b*) and 2(*a*) show the stability diagram for $A = 0.9$ and $A = 0.8$, respectively. The stability curves for these two cases have the same

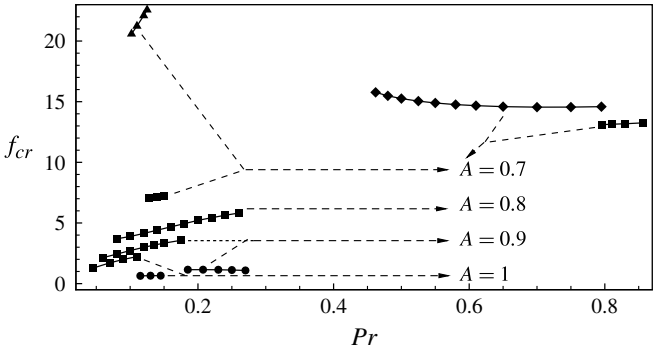

FIGURE 3. Critical frequency f_{cr} versus the Prandtl number. Solid circles (●), $m = 2$ modes at the transition; solid squares (■), $m = 3$ modes; solid diamonds (◆), $m = 4$ modes; solid up triangles (▲), $m = 6$ modes.

topology, and both of them are different from that of $A = 1$. The critical points for the axisymmetric flows beyond the second bifurcation no longer form a closed curve. The critical curves exhibit an 'S' shape. As can be seen in figure 1(*b*), the stability curve for $A = 0.9$, the axisymmetric flow beyond the second bifurcation exists for $0.05 \leqslant Pr \leqslant 0.9$, and it becomes a steady $m = 2$ flow with decreasing Ra. Moreover, the critical points connect with the second bifurcation points at Pr around 0.9, which is different from that of $A = 1$. With increasing Ra, the mode changes for $A = 1$ and $A = 0.9$ are identical to the variation in the Prandtl number. The critical curve for $A = 0.8$, shown in figure 2(*a*), is slightly different from that of the $A = 0.9$ case. The axisymmetric flow loses stability to steady $m = 2$ flow with decreasing Ra for $0.053 \leqslant Pr \leqslant 0.47$, where the Prandtl number range for this transition is much shorter than that of $A = 0.9$. Unlike the previous two cases, the oscillatory $m = 2$ mode no longer exists. Instead, a steady $m = 8$ mode is obtained, which is not found for the last two aspect ratios.

Figure 2(*b*) shows the stability diagram for $A = 0.7$. No axisymmetric flow was found beyond the second bifurcation. Our finding is that frequent changes of instability mode occur when Pr is changed. The primary axisymmetric flow loses stability to a series of steady or unsteady three-dimensional flows with increasing Ra. It can be seen from the figure that the critical mode with respect to the second bifurcation for small Prandtl number is steady for $m = 2$. With increasing Pr, the most unstable mode becomes oscillatory for $m = 6$, oscillatory for $m = 3$, steady for $m = 8$, steady for $m = 9$, steady for $m = 10$, oscillatory for $m = 4$, oscillatory for $m = 3$, steady for $m = 1$. The critical Rayleigh number increases with increasing Pr for $0.02 \leqslant Pr < 0.3$ and grows especially rapidly for $0.05 \leqslant Pr \leqslant 0.126$. It decreases with further increase in Pr for $0.3 \leqslant Pr \leqslant 1$.

The critical frequency corresponding to the oscillatory critical mode is $f_{cr} = \omega_{cr}/2\pi$, where ω_{cr} is the angular frequency. The dependence of critical frequency on Prandtl number is shown in figure 3. It is observed that the frequencies increase as Pr increases for $m = 3$ modes, and is almost unchanged for $m = 2$ modes. The frequencies increase steeply with increase in Pr for $m = 6$ modes, and decrease gradually to a constant value for $m = 4$ modes. The frequencies for smaller-aspect-ratio cylinders are higher than those for larger-aspect-ratio cylinders.

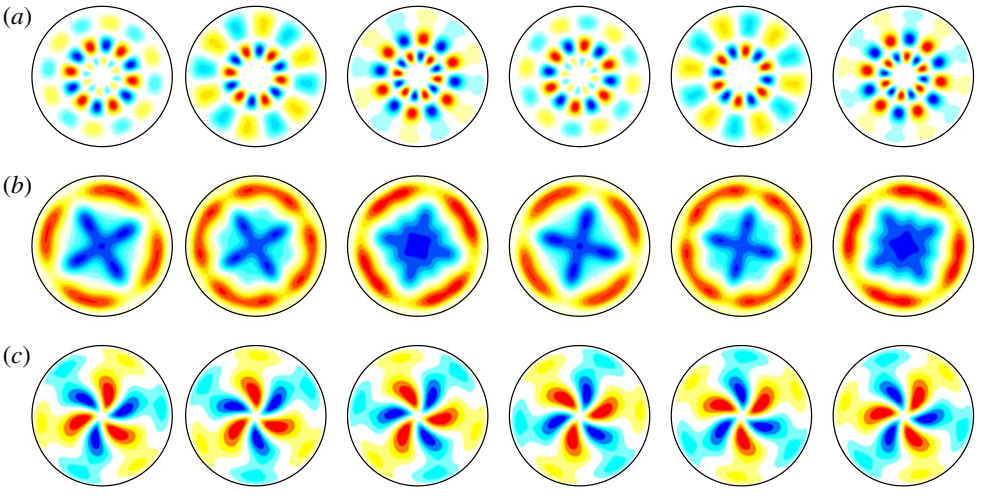

FIGURE 4. (Colour online) Nonlinear simulation of periodic flows for $A = 0.7$ at $t = 0, T/6, 2T/6, \ldots$. (*a*) Standing waves at $Pr = 0.11$, $Ra = 83\,000$, contours of azimuthal velocity on the $z = 0.6$ plane; (*b*) standing waves at $Pr = 0.7, Ra = 80\,000$, contours of vertical velocity on the $z = 0.6$ plane; (*c*) travelling waves at $Pr = 0.82, Ra = 77\,000$, contours of azimuthal velocity on the $z = 0.5$ plane.

The stability results show the transition from axisymmetric flow to three-dimensional flow via two types of symmetry-breaking bifurcation. The instability-breaking $O(2)$ symmetry is either due to steady bifurcation or due to Hopf bifurcation. As can be seen from the stability results, there are very rich symmetry-breaking phenomena. The steady state is reflection-symmetric in the azimuthal direction and the reflection symmetry is broken by subsequent bifurcation. The periodic solutions have the form of travelling waves or standing waves, where the travelling waves preserve space–time symmetry and the standing wave preserves a purely spatial reflection symmetry. We have performed several nonlinear simulations to determine whether the periodic solution near onset is a travelling or standing wave. Three periodic flows for $A = 0.7$ are presented in figure 4. A standing wave flow was found at $Pr = 0.11$, $Ra = 83\,000$ with wavenumber $m = 6$, as shown in figure 4(*a*). The flow at $Pr = 0.7$, $Ra = 80\,000$ with wavenumber $m = 4$ is also a standing wave solution, as shown in figure 4(*b*). Travelling waves were found for $m = 3$ flows for both lower and higher ranges of Prandtl number. We have plotted the travelling waves at $Pr = 0.82$, $Ra = 77\,000$ in figure 4(*c*).

Finally, the effect of the aspect ratio ($0.67 \leqslant A \leqslant 1.1$) is studied for $Pr = 0.1$. The critical Rayleigh numbers are given as a function of A in figure 5. It can be seen that the stability curve is folded in some aspect ratio range. For $0.67 \leqslant A < 0.75$ the axisymmetric flow loses stability to three different states (steady $m = 2$, oscillatory $m = 6$ and oscillatory $m = 3$). For larger values of A ($0.75 \leqslant A < 1.1$), the stability curve exhibit an 'anti-S' shape. Beyond the second bifurcation, there exists a linearly stable region of Rayleigh numbers for $0.75 \leqslant A \leqslant 1.05$ within which either a decrease or increase in Ra will cause three-dimensional convection. The transition of this flow with increasing Ra corresponds to an oscillatory $m = 3$ mode and a steady $m = 1$ mode in certain Pr ranges. Moreover, the transition corresponds to a steady $m = 2$ mode with decreasing Ra.

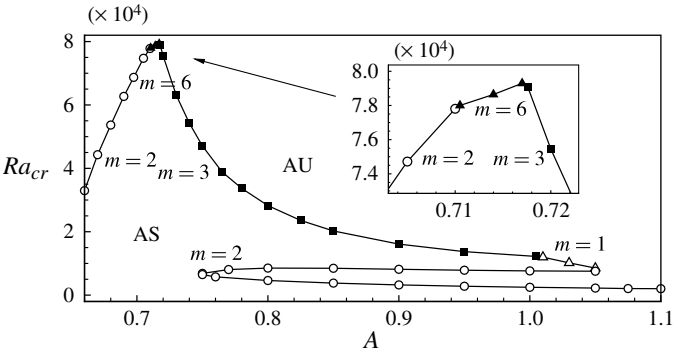

FIGURE 5. Critical Rayleigh number Ra_{cr} as a function of aspect ratio A for $Pr = 0.1$. Solid curves with hollow symbols represent steady transitions and solid symbols oscillatory transitions. Up triangles (△), $m = 1$ modes at the transition; circles (○), $m = 2$ modes; solid squares (■), $m = 3$ modes; solid up triangles (▲), $m = 6$ modes. The AS in the figures indicates the region in which the axisymmetric flow is stable, and AU means there is no stable axisymmetric base flow in the region.

3.2. *Energy analysis*

To investigate the physical mechanism responsible for the stability of the axisymmetric flow, a kinetic energy transfer budget was performed for a fixed Prandtl number $Pr = 0.1$, and Rayleigh numbers near the three critical points ($Ra = 2460, 7650, 12\,350$). Figure 6(*a*) shows the result given by the energy analysis for the second bifurcation. As we can see, the basic solution becomes unstable first at $Ra = 2460$. For $Ra > 2460$, both inertial term K_{v2} and buoyancy term K_b are growing, being responsible for the instability. Figure 6(*b*) shows the rate of change of energy for the destabilization process of the axisymmetric flow with decreasing Ra. The increase of inertial term K_{v2} and buoyancy term K_b cause the destabilized effect. The flow bifurcates to a steady $m = 2$ flow. Note that K_{v3} increases as the Rayleigh number increases up to 7650. Figure 6(*c*) gives the results of the kinetic energy fluctuation analysis for transition to an oscillatory state. This oscillatory state beyond the threshold is decomposed into its mean value in time and the oscillatory fluctuations as basic states and perturbations; similarly, equation (2.9) is used to perform kinetic transfer analysis. We consider $Ra = 12\,350$, which is slightly above the oscillatory threshold $Ra_{cr} = 12\,300$. It is clear from this figure that the previous increasing term K_{v3} becomes dominantly destabilizing. Combined with the buoyancy term K_b, both of these terms contribute to the transition. Incidentally, the energy budget for higher Rayleigh numbers, which is not plotted here, shows that K_{v3} grows and becomes much larger than K_b.

Kinetic energy transfer analyses are also performed for $A = 0.7$ and Prandtl number equal to 0.12, 0.4 and 0.6. The critical mode for $Pr = 0.12$ is periodic for $m = 6$, and the corresponding kinetic energy fluctuation analysis at $Ra = 90\,600$ (just above the oscillatory threshold $Ra_{cr} = 90\,500$) is shown in figure 7. Here K_{v2} is still the leading destabilizing term, K_{v3} is the second destabilizing term, and the effect of K_b is weaker than the previous two. Thus, the instability here is mainly due to inertial mechanisms. The critical mode for $Pr = 0.4$ is steady for $m = 10$; the kinetic transfer analysis (figure 7*b*) obviously demonstrates that the flow bifurcation is caused by the buoyancy effect. Lastly, for $Pr = 0.6$ with periodic critical mode $m = 4$, the kinetic energy fluctuation analysis performed at $Ra = 84\,200$(critical Rayleigh number $Ra_{cr} = 84\,000$)

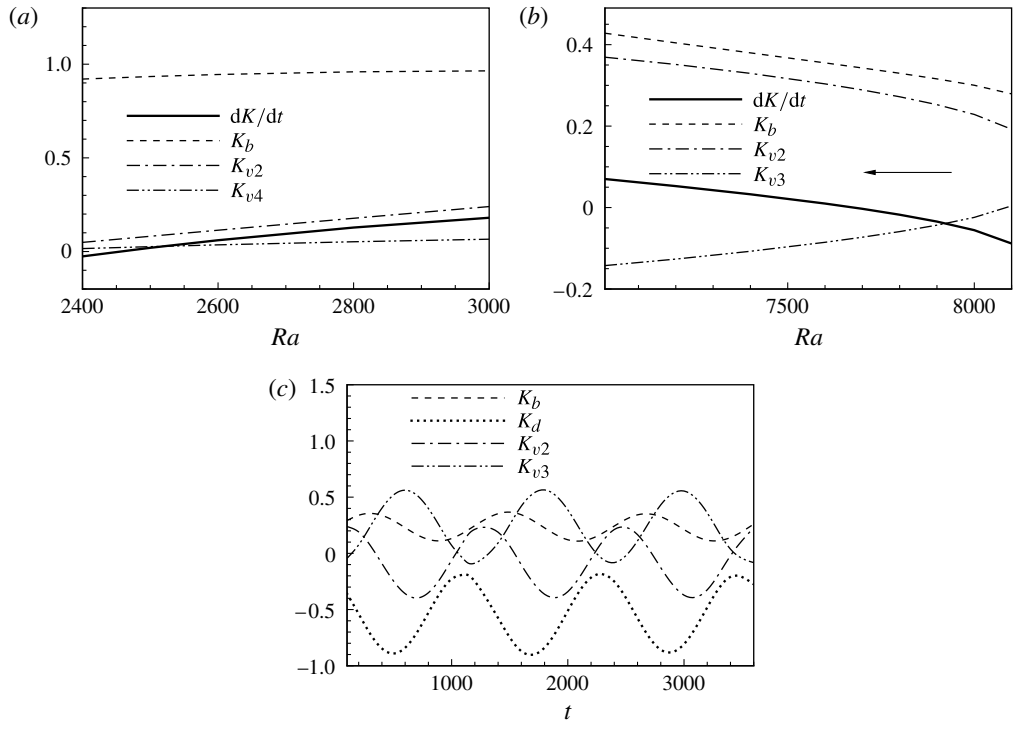

FIGURE 6. Perturbation kinetic energy contributions for (*a*) *Ra* around 2460, (*b*) *Ra* around 7650, and (*c*) $Ra = 12\,350$ at fixed $A = 1$, $Pr = 0.1$.

is shown in figure 7. The buoyancy term K_b and inertial term K_{v2} are close in amplitude, and the instability is due to the combination of the two mechanisms.

In summary, energy analysis for $A = 1$, $Pr = 0.1$ (figure 6) shows both inertial term K_{v2} and buoyancy term K_b contributions to the steady transition of the axisymmetric flow. The inertial term K_{v3} is responsible for the oscillatory transition. Energy analysis for $A = 0.7$ (figure 7) shows that the inertial term K_{v2} and the inertial term K_{v3} are the leading destabilizing terms for the oscillatory transition at $Pr = 0.12$, the inertial term K_{v2} and the buoyancy term K_b are the leading destabilizing terms for the oscillatory transition at $Pr = 0.6$, and the buoyancy term K_b is the leading destabilizing term for the high-wavenumber steady transition. Now K_{v2} measures the amplification of radial velocity disturbance (u_r') by axial transport (u_z') of axial gradients of the basic radial flow ($\partial_z u_r$), and K_{v3} describes the amplification of the axial velocity disturbance (u_z') by radial transport (u_r') of axial shear ($\partial_r u_z$) (Wanschura *et al.* 1996). Hence the axial shear of mean flow is more significant for oscillatory transitions in a relatively tall cylinder ($A = 1$), while the radial shear of mean flow is more important for oscillatory transition in a relatively short cylinder ($A = 0.7$).

Previously the literature (Wanschura *et al.* 1996; Touihri *et al.* 1999; Gelfgat, Bar-Yoseph & Solan 2000; Ma *et al.* 2005) has shown that for low-Prandtl-number fluids ($Pr = 0.02$) the flow becomes oscillatorily unstable due to inertial mechanisms. For high-Prandtl-number fluids ($Pr = 1$) the flow becomes unstable due to thermal mechanisms. In a relatively short cylinder, the flow tends to be oscillatorily unstable, while in a tall cylinder the flow tends to be unstable via steady bifurcation. There must

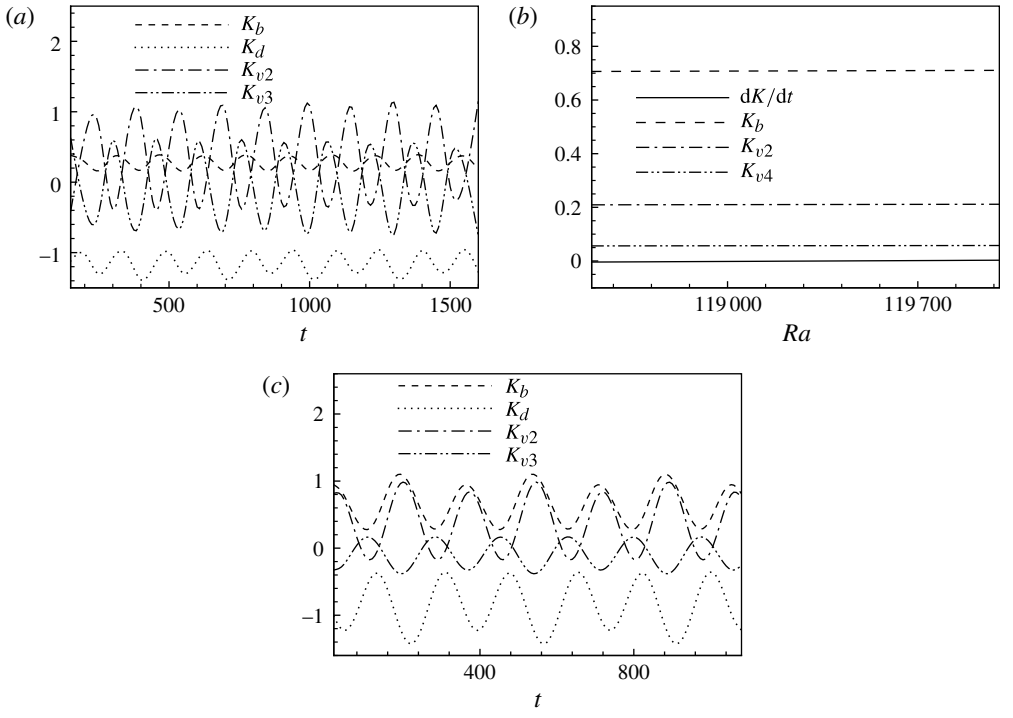

FIGURE 7. Perturbation kinetic energy contributions for (*a*) $Ra = 90\,600$ and $Pr = 0.12$, (*b*) Ra around 119 000 and $Pr = 0.4$, and (*c*) $Ra = 84\,200$ and $Pr = 0.6$ at fixed $A = 0.7$.

be some transition range for both Prandtl number and aspect ratio. The parameters we have studied ($A = 1, 0.9, 0.8, 0.7, 0 < Pr < 1$) are included in the transition range. The instability properties are more complicated in this region. The transition range for A can be found in figure 5. It can be speculated that the whole critical surface is partially multi-valued and continuous, but folded in such a way that a cusp develops. This phenomenon often occurs due to competition between different instability mechanisms.

Further, the boundaries of a flow are an important factor. They constrain the development of a disturbance, and usually, the closer they are together the more stable the flow. However, they sometimes give rise to strong shear in boundary layers which is diffused outwards by viscosity and so leads to instability of the flow.

4. Conclusion

The stability of steady axisymmetric convection in a vertical cylinder heated from below has been presented in this paper, which indicates that stability properties depend strongly on cylinder geometry and the Prandtl number. For $A = 1$, there is a closed parameter region for stable axisymmetric flow beyond the second bifurcation. For $A = 0.8$ and $A = 0.9$, the region is no longer closed. The stability curves exhibit an 'S' shape, which means that the primary axisymmetric flow connects with the second axisymmetric flow. However, for $A = 0.7$ no axisymmetric flow is found beyond the second bifurcation. The particular shape of the stability boundary is due to the effect of different instability mechanisms, i.e. the Rayleigh–Bénard mechanism (buoyancy K_b) and inertial mechanisms (radial shear K_{v2} and axial shear K_{v3} of base flow).

The flow in tall cylinders loses stability due to the buoyancy mechanism, which is connected with the axial shear of the basic flow, and loses stability due to radial shear of basic flow in short cylinders. For $A = 0.7$ the flow loses stability to multiple modes for different Prandtl numbers, which is also the result of the interaction of several mechanisms. There is a moderate-aspect-ratio region in which several instability mechanisms work together.

Acknowledgements

This work was supported by the National Natural Science Foundation of China under Grants 11072238 and 10602056, and the 111 Project of China under Grant B07033.

REFERENCES

BODENSCHATZ, E., PESCH, W. & AHLERS, G 2000 Recent developments in Rayleigh–Bénard convection. *Annu. Rev. Fluid Mech.* **32**, 709–778.

BOROŃSKA, K. & TUCKERMAN, L. S. 2006 Standing and travelling waves in cylindrical Rayleigh–Bénard convection. *J. Fluid Mech.* **559**, 279–298.

BOROŃSKA, K. & TUCKERMAN, L. S. 2010*a* Extreme multiplicity in cylindrical Rayleigh–Bénard convection. Part 1. Time-dependence and oscillations. *Phys. Rev.* E **81**, 036320.

BOROŃSKA, K. & TUCKERMAN, L. S. 2010*b* Extreme multiplicity in cylindrical Rayleigh–Bénard convection. Part 2. Bifurcation diagram and symmetry classification. *Phys. Rev.* E **81**, 036321.

BUELL, J. C. & CATTON, I. 1983 The effect of wall conduction on the stability of a fluid in a right circular cylinder heated from below. *Trans. ASME: J. Heat Transfer* **105**, 255–260.

CHARLSON, G. S. & SANI, R. L. 1970 Thermoconvective instability in a bounded cylindrical fluid layer. *Intl J. Heat Mass Transfer* **13**, 1479–1496.

CHARLSON, G. S. & SANI, R. L. 1971 On thermoconvective instability in a bounded cylindrical fluid layer. *Intl J. Heat Mass Transfer* **14**, 2157–2160.

CHARLSON, G. S. & SANI, R. L. 1975 Finite amplitude axisymmetric thermoconvective flows in a bounded cylindrical layer of fluid. *J. Fluid Mech.* **71**, 209–229.

CROSS, M. C. & HOHENBERG, P. C. 1993 Pattern formation outside of equilibrium. *Rev. Mod. Phys.* **65**, 851–1112.

GELFGAT, A. Y., BAR-YOSEPH, P. Z. & SOLAN, A. 2000 Axisymmetry breaking instabilities of natural convection in a vertical bridgman growth configuration. *J. Cryst. Growth* **220**, 316–325.

HARDIN, G. R. & SANI, R. L. 1993 Buoyancy-driven instability in a vertical cylinder: binary fluids with Soret effect. Part 2. Weakly nonlinear solutions. *Intl J. Numer. Meth. Fluids* **17** (9), 755–786.

HÉRT, F., HUFSCHMID, R., SCHEEL, J. & AHLERS, G. 2010 Onset of Rayleigh–Bénard convection in cylindrical containers. *Phys. Rev.* E **81**, 046318.

HOF, B., LUCAS, P. G. L. & MULLIN, T. 1999 Flow state multiplicity in convection. *Phys. Fluids* **11** (10), 2815–2817.

HUGUES, S. & RANDRIAMAMPIANINA, A. 1998 An improved projection scheme applied to pseudospectral methods for the incompressible Navier–Stokes equations. *Intl J. Numer. Meth. Fluids* **28**, 501–521.

KNOLL, D. A. & KEYES, D. E. 2004 Jacobian-free Newton–Krylov methods: a survey of approaches and applications. *J. Comput. Phys.* **193**, 357–397.

LEHOUCQ, R. B., SORENSEN, D. C. & YANG, C. (Eds) 1998 *ARPACK Users Guide: Solution of Large-Scale Eigenvalue Problems with Implicitly Restarted Arnoldi Methods*. SIAM.

LEONG, S. S. 2002 Numerical study of Rayleigh–Bénard convection in a cylinder. *Numer. Heat Transfer* A **41**, 673–683.

MA, D. J., HENRY, D. & BEN HADID, H. 2005 Three-dimensional numerical study of natural convection in vertical cylinders partially heated from the side. *Phys. Fluids* **17**, 124101.

MA, D. J., SUN, D. J. & YIN, X. Y. 2006 Multiplicity of steady states in cylindrical Rayleigh–Bénard convection. *Phys. Rev.* E **74**, 037302.

MÜLLER, G., NEUMANN, G. & WEBER, W. 1984 Natural convection in vertical Bridgman configurations. *J. Cryst. Growth* **70**, 78–93.

NEUMANN, G. 1990 Three-dimensional numerical simulation of buoyancy-driven convection in vertical cylinders heated from below. *J. Fluid Mech.* **214**, 559–578.

ROSENBLAT, S. 1982 Thermal convection in a vertical circular cylinder. *J. Fluid Mech.* **122**, 395–410.

RÜDIGER, S. & FEUDEL, F. 2000 Pattern formation in Rayleigh–Bénard convection in a cylindrical container. *Phys. Rev.* E **62**, 4927–4931.

STORK, K. & MÜLLER, U. 1975 Convection in boxes: an experimental investigation in vertical cylinders and annuli. *J. Fluid Mech.* **71**, 231–240.

TOUIHRI, R., BEN HADID, H. & HENRY, D. 1999 On the onset of convective instabilities in cylindrical cavities heated from below. Part 1. Pure thermal case. *Phys. Fluids* **11**, 2078–2088.

TUCKERMAN, L. S. & BARKLEY, D. 2000 Bifurcation analysis for time steppers. In *Numerical Methods for Bifurcation Problems and Large-Scale Dynamical Systems* (ed. E. Doedel & L. S. Tuckerman), vol. 119, pp. 453–466. Springer.

VERZICCO, R. & ORLANDI, P. 1996 A finite-difference scheme for the three-dimensional incompressible flows in cylindrical coordinates. *J. Comput. Phys.* **123**, 402–414.

VAN DER VORST, H. A. 1992 BI-CGSTAB: a fast and smoothly converging variant of BI-CG for the solution of nonsymmetric linear systems. *SIAM J. Sci. Stat. Comput.* **13**, 631–644.

WANSCHURA, M., KUHLMANN, H. C. & RATH, H. J. 1996 Three-dimensional instability of axisymmetric buoyant convection in cylinders heated from below. *J. Fluid Mech.* **326**, 399–415.